Three-dimensional dynamics of tidal front and cross-front nutrients transport

Menghong Dong[1], Xinyu Guo[2]

[1]*State Key Laboratory of Satellite Ocean Environment Dynamics, Second Institute of Oceanography, Ministry of Natural Resources, Hangzhou, 310012, China*

[2]*Center for Marine Environmental Studies, Ehime University, Matsuyama, 7908577, Japan*

Purposes

A front is formed when two different water masses converge and there are many types of fronts exist in the shelf sea. Tidal fronts form in the transition area between vertical mixed water and stratified water, caused by tidal stirring and surface heating, respectively, and primarily occur in summer (Simpson & Hunter, 1974; Yanagi, 1987). Utilizing high-resolution satellite observational data, Dong and Guo (2021) found that the intra-tidal movement of the tidal front in Bungo Channel is significant, and is mainly controlled by tidal current advection. Notably, the intensity of the front increases during the ebb current phase, which carries the front toward the stratified area, but decreases during the flood current phase which drives the front in the opposite direction. In the field observational data, we found that during the intra-tidal movement of the front, not only the intensity but also the vertical structure of the front changed. When the front approaches the stratified or mixed area, the front becomes steeper or flattened respectively in the vertical direction. However, the dynamic mechanisms of these changes are not clear and need to be clarified utilizing numerical model studies.

In addition, high biological production in the frontal zone is always related to the nutrient supply across the front (Takeoka, 2002). However, the cross-front transport process is difficult to directly observe, and it is also unclear what impact changes in frontal strength or structure will have on the transport during the movement of the front. This also requires numerical studies to reproduce the cross-front nutrient transport processes and quantify the associated fluxes.

The current project focuses on the three-dimensional dynamics of tidal front and the cross-front transport of nutrients through a numerical study. We first constructed a non-hydrostatic, three-dimensional numerical model to explore the mechanisms of the front variations during its movement, and then added a particle tracer to the model to simulate the cross-front transport process of nutrients.

Methods

We used the general circulation model developed at the Massachusetts Institute of Technology (MITgcm) (Marshall et al., 1997) as our numerical model to explore the variations of a simulation tidal front and its mechanism. MITgcm has a dynamic kernel that can drive either oceanic or atmospheric simulations and has non-hydrostatic capabilities, allowing the model to address a wide range of phenomena from convection to global circulation patterns (Adcroft et al., 2021). The model

uses a finite volume method with an Arakawa C grid for spatial discretization and z coordinates in the vertical direction (Arakawa & Lamb, 1977). The model can be efficiently applied on a wide variety of computational platforms.

The numerical model used in this study was configured in a 160 × 50 km channel with a flat bottom (75 m depth) and had a spatial resolution of 1 km in both the x and y directions. There are 25 layers in the vertical direction with a constant thickness of 3 m. The periodic condition connecting the numerical solution at both ends (x = 0 and 160 km) and the no-slip boundary conditions at y = 0 and 50 km were adopted in the x and y directions, respectively. At x = 80 km, the channel narrows to 12 km to simulate a strait, aiming to induce strong vertical mixing. The model forcing includes heat flux and tidal currents represented by only one tidal constituent, S2. The heat flux entering the ocean through the sea surface is 120 Wm^{-2}. The amplitude of the tidal current at both the east and west open boundaries is 0.2 m/s, and the phase difference calculated using the shallow water wave phase velocity is 1.64 hours (the tidal current at the east boundary is ahead of the tidal current at the west boundary). An idealized thermocline is initially uniformly set in the horizontal direction, and the temperature change from 15 ℃ at the surface to 5 ℃ at the bottom. The initial salinity is 35 psu and is uniformly distributed throughout the field. The model time step is 10 s and the integration is performed over 20 days. The results from the last 12 hours of the model, which correspond to one tidal cycle, are used for analysis.

Results

Figures 1 and 2 show the changes in the SST and its gradient near the strait over one tide cycle. The vicinity of the strait is a mixed area with an SST of approximately 8°C, while areas farther from the strait form a stratified region with an SST of approximately 20°C (Figure 1). The middle zone, characterized by a large temperature gradient, is the tidal front. During the ebb current phase, when the tidal current flowed eastward (from 00:00 to 06:00), the tidal front shifted approximately 5 km eastward into the stratified area (from x = 87 km to 92 km), during which the intensity of the front (measured by the temperature gradient) increased from ~2 to ~4°C/km. In contrast, during the flood current phase, when the tidal current flowed westward (from 06:00 to 11:00), the tidal front gradually moved back toward the west into the mixed area, while its intensity decreased. The intra-tidal variations in the position and intensity of the tidal front at the sea surface were consistent with those observed in satellite SST data (Dong & Guo, 2021).

We then performed particle tracking to verify whether the movement of the front was entirely controlled by tidal current advection. At 00:00, we released a batch of particles at the front to track their movement over one tidal cycle. When the front shifted from the mixed to the stratified area (from 00:00 to 06:00), its movement closely matched that of the particles (Figure 2). However, when the front returned from the stratified to the mixed area (from 06:00 to 11:00), it moved less than the

particles (Figure 2). This discrepancy may have occurred because vertical mixing was stronger closer to the strait. Therefore, when the buoyancy input from horizontal advection no longer exceeds the vertical mixing power during movement into the mixed area, the front ceases to advance further.

In addition, we calculated the Simpson and Hunter (1974) parameter $log_{10}(H/u^3)$, where H is water depth (m) and u is the amplitude of the tidal current (ms^{-1}) (Figure 2). According to the energetics framework provided by Simpson and Hunter (1974), tidal fronts align along the contour of a critical value of this parameter. In our model results, the critical value at the tidal front area ranged between 2.5 and 3.5, which is consistent with values reported in the Seto Inland Sea (Yanagi & Okada, 1993).

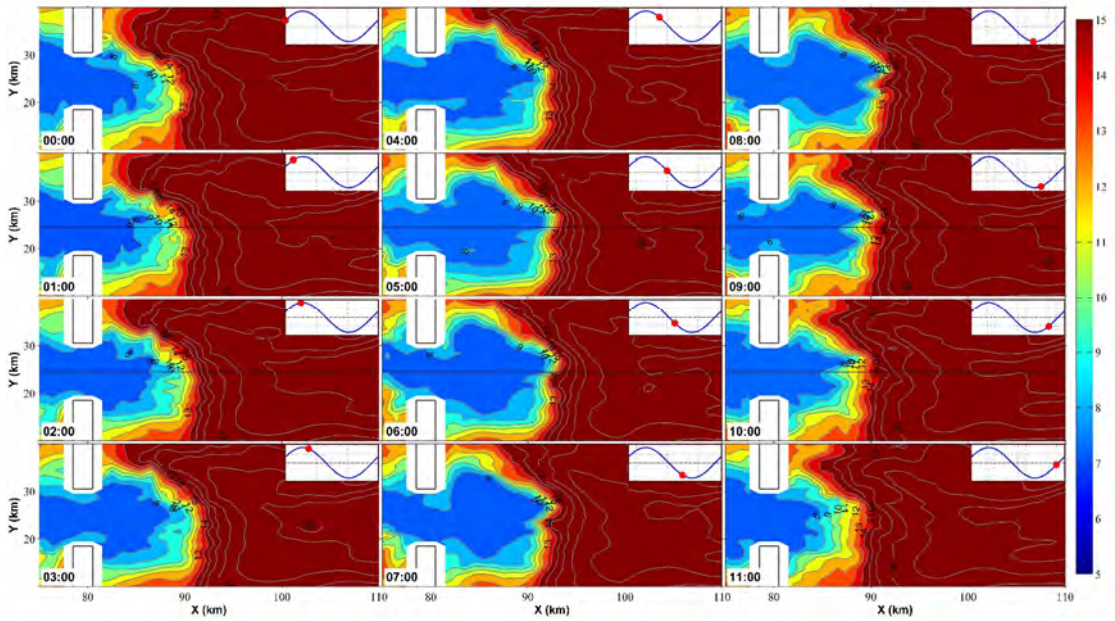

Figure 1. Changes in the simulated SST near the strait over one tide cycle (00:00 to 11:00). The blue line indicates the time series of the tidal current at the eastern boundary.

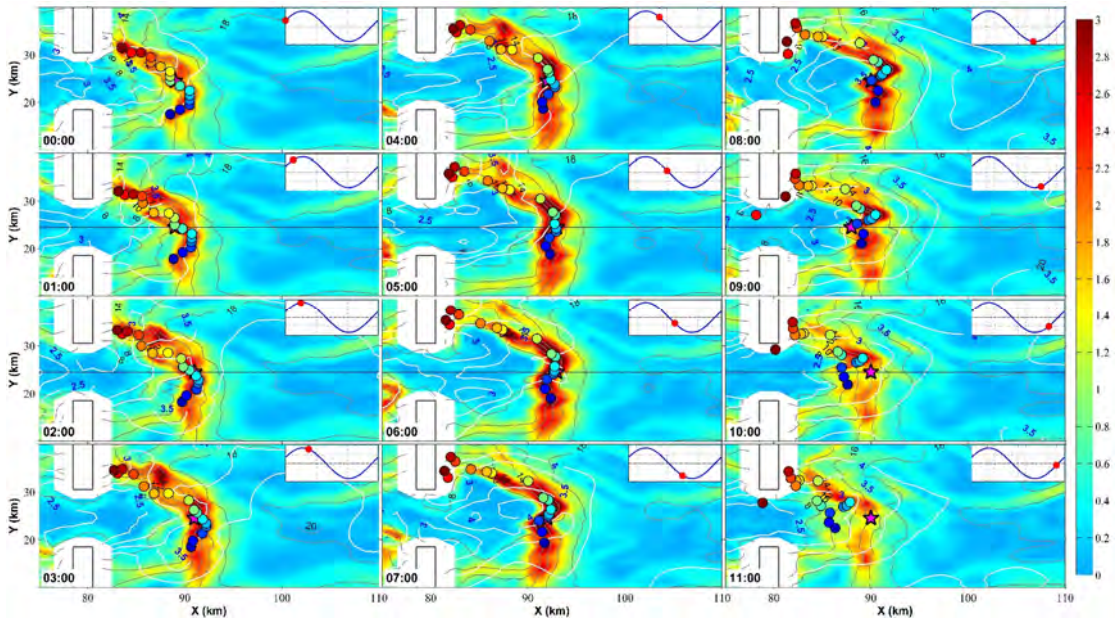

Figure 2. Changes in the gradient of the simulated SST near the strait over one tide cycle. White

lines indicate the calculated Simpson and Hunter (1974) parameter $log_{10}(H/u^3)$, where H is the water depth (m) and u is the amplitude of the tidal current (ms^{-1}). At 00:00, a batch of color-differentiated particles was released at the front to track their movement along with the front. The pink star represents the frontal position at y=25.

The changes in the vertical structure of the tidal front and the vertical eddy viscosity around the front are shown in Figures 3 and 4. Near slack tide, when the tidal current transitioned from flood current to ebb current (00:00 and 11:00 in Figure 3), the tidal front was relatively flat in the vertical direction. Conversely, near another slack tide, when the tidal current changed from ebb current to flood current (05:00 and 06:00 in Figure 3), the tidal front became steeper in the vertical direction. During the ebb current phase (00:00 to 06:00), because the current velocity near the strait was larger than that farther from the strait, a convergence occurred near the front, increasing its intensity as it moved into the stratified area (Figure 3). However, when the heavy water from the mixed area was brought to the stratified area, convective instability occurred, enhancing vertical mixing as vertical eddy viscosity increased (Figure 4). Consequently, the tidal front became steeper in the vertical direction (Figure 3).

During the flood current phase (06:00 to 11:00), a divergence occurred near the tidal front, also due to the current velocity near the strait being larger than that farther from the strait. The intensity of the front then decreased as the front moved into the mixed area (Figure 3). Simultaneously, the light water from the stratified area was advected to the mixed area, remaining above the denser water, which weakened vertical mixing as vertical eddy viscosity decreased (Figure 4). As a result, the tidal front stretched and flattened in the vertical direction (Figure 3). The processes in which dense water moved into the stratified area and enhanced vertical mixing during the ebb current phase, and in which lighter water sheared and floated over the dense water to suppress vertical mixing during the flood current phase, are characteristic of tidal straining.

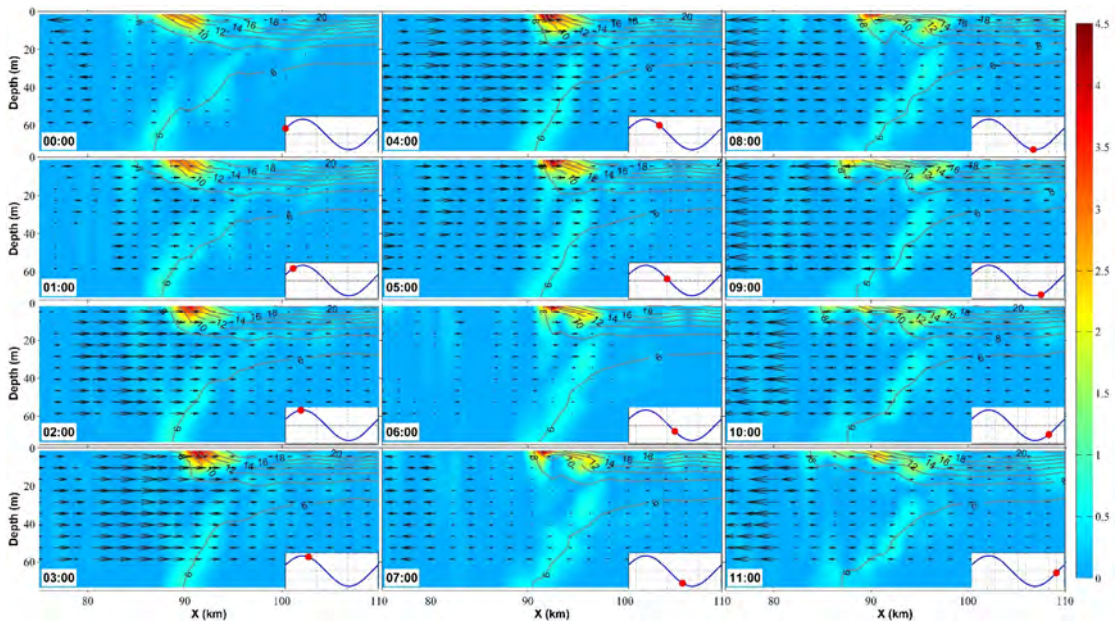

Figure 3. Changes in the along-channel vertical structure (at y=25) of the tidal front over one tide cycle. Contours indicate temperature and colors indicate the magnitude of the horizontal temperature gradient. Arrows indicate the eastward component of the tidal current.

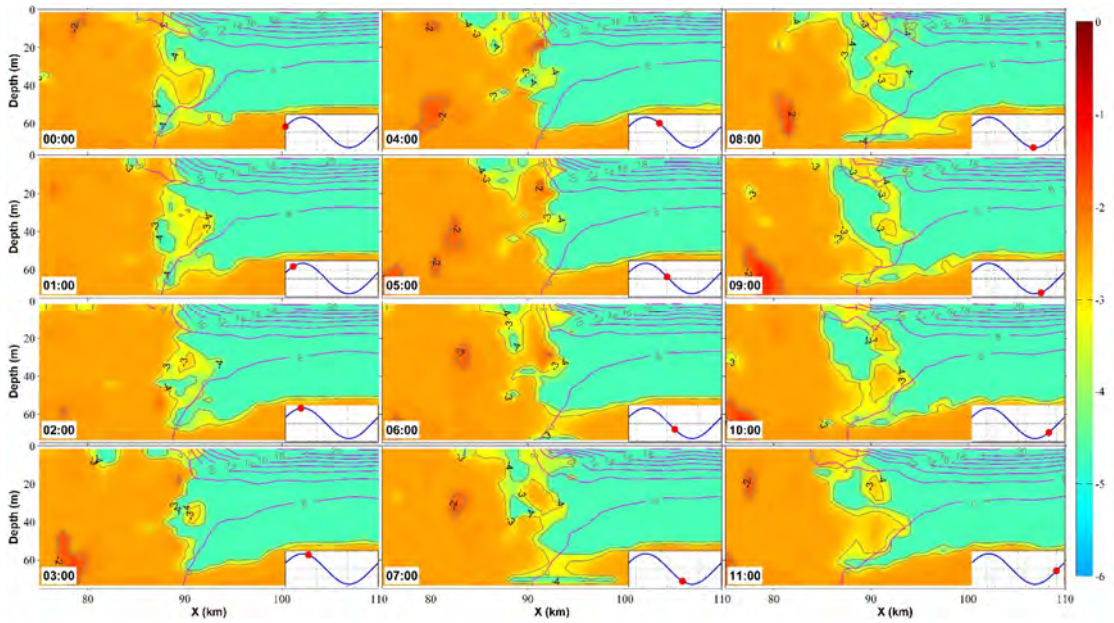

Figure 4. Changes in the along-channel vertical section (at y=25) of vertical eddy viscosity (colors) around the front over one tide cycle. Contours indicate temperature.

Regarding particle movement throughout the water column, when the front moves from the stratified area to the mixed area under the influence of tidal currents, particles in the stratified area are carried into the mixed region and undergo vertical mixing. Notably, in the opposite process—when the front moves from the mixed area to the stratified area—particles in the mixed region tend to enter the middle layer of the stratified region rather than remain in the same horizontal layer. This is because the density of the water in the mixed area is between that of the upper and lower layers in the stratified region, causing the mixed water to intrude into the middle layer of the stratified region, while the water from the upper and lower layers flows into the mixed area. Consequently, nutrient-rich water in the lower layer can be transported to the upper layer via the mixed region. This process aligns with the "nutrient bypass" mechanism for nutrient transport in frontal zones previously proposed by Takeoka (2002).

Future challenges

We have used an idealized model to gain a general understanding of cross-frontal nutrient transport in this study. However, to quantitatively evaluate transport fluxes and their contribution to marine primary productivity, it is still necessary to develop a numerical model that simulates real ocean conditions. In the future, we plan to establish a high-resolution three-dimensional coupled physical-ecosystem model for the tidal front in the Bungo Channel, aiming to comprehensively assess cross-

frontal nutrient transport and its impact on marine productivity.

Publications

Dong, M., & Guo, X. (2024). Multiple timescale variations in fronts in the Seto Inland Sea, Japan. Ocean Science, 20, 1527‑1546. https://doi.org/10.5194/os-20-1527-2024

References

Adcroft, A., Campin, J.-M., Doddridge, E., Dutkiewicz, S., Evangelinos, C., Ferreira, D., et al. (2021). *MITgcm user manual*. Retrieved from https://mitgcm.readthedocs.io/en/latest/overview/overview.html

Arakawa, A., & Lamb, V. R. (1977). *Computational Design of the Basic Dynamical Processes of the UCLA General Circulation Model*. *METHODS IN COMPUTATIONAL PHYSICS: Advances in Research and Applications: Volume 17: General Circulation Models of the Atmosphere* (Vol. 17). ACADEMIC PRESS, INC. https://doi.org/10.1016/b978-0-12-460817-7.50009-4

Dong, M., & Guo, X. (2021). The intra-tidal characteristics of tidal front and their spring–neap tidal and seasonal variations in bungo channel, Japan. *Remote Sensing*, *13(9)*(9), 1840–1859. https://doi.org/10.3390/rs13091840

Marshall, J., Adcroft, A., Hill, C., Perelman, L., & Heisey, C. (1997). A finite-volume, incompressible navier stokes model for, studies of the ocean on parallel computers. *Journal of Geophysical Research C: Oceans*, *102*(C3), 5753–5766. https://doi.org/10.1029/96JC02775

Simpson, J. H., & Hunter, J. R. (1974). Fronts in the Irish Sea. *Nature*, *250*, 404–406. https://doi.org/10.1038/250404a0

Takeoka, H. (2002). Progress in Seto Inland Sea Research. *Journal of Oceanography*, *58(1)*(1), 93–107. https://doi.org/10.1023/A:1015828818202

Yanagi, T. (1987). Classification of “Siome”, Streaks and Fronts. *Journal of the Oceanographical Society of Japan*, *43*(3), 149–158. https://doi.org/10.1007/BF02109215

Yanagi, T., & Okada, S. (1993). Tidal fronts in the Seto Inland Sea. *Mem. Fac. Eng. Ehime Univ.*, *12*(4), 337–343.